Supporting Information

Tuning the electrochemical performance of Ti_3C_2 and Hf_3C_2 monolayer by functional groups for metal-ion batteries application

Zhifang Yang,[a] Yanping Zheng,[b] Wenliang Li,*[a] Jingping Zhang*[a]

a. Faculty of Chemistry, National & Local United Engineering Laboratory for Power Batteries, Northeast Normal University, Changchun 130024, China;

b. Faculty of Chemistry, Tonghua Normal University, Tonghua, 134002, China.

E-mail: jpzhang@nenu.edu.cn; liwl926@nenu.edu.cn

Table of contents

Computational Details

The surface energy (γ)[1] of configuration I are considered, which is listed in Table S2. The corresponding surface energy is defined as:

$$\gamma = \frac{E_{iso} - N_L \sigma_{bulk}}{2A}$$

The exfoliation energy (E_{exf})[2] per unit area can be obtained exactly as the ground state energy difference between a bulk material and a single isolated layer, expressed as:

$$E_{exf} = \frac{E_{iso} - E_{bulk}}{A}$$

where E_{iso} and E_{bulk} denote the total energies of the primitive cell of an isolated slab and a bulk system, respectively. N_L is the total number of atoms in the slab, A is the area of the bottom or top face of the slab, and σ_{bulk} is the energy per atom in the bulk crystal.

Supporting Figures

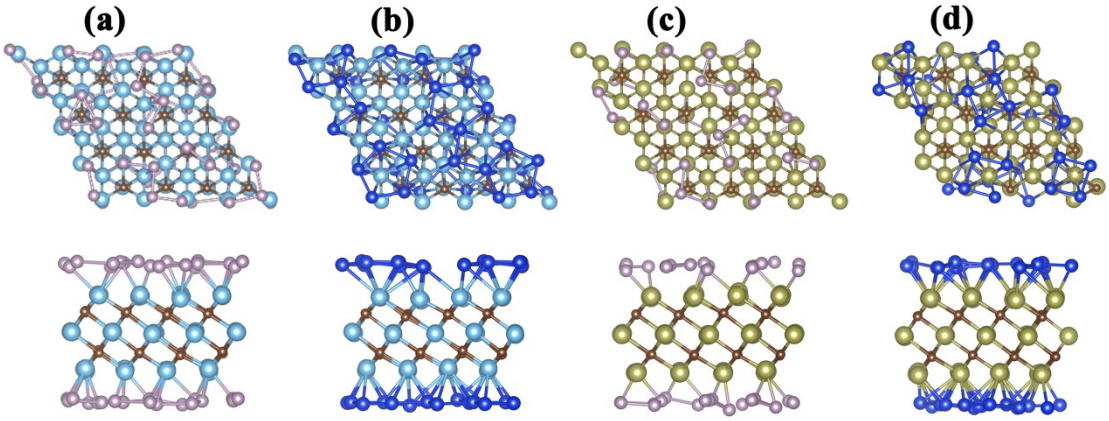

Fig. S1 Snapshots of the final frame of I-$Ti_3C_2X_2$ and I-$Hf_3C_2X_2$ (X = Si, and P) monolayer at 300 K, (a) I-$Ti_3C_2P_2$, (b) I-$Ti_3C_2Si_2$, (c) I-$Hf_3C_2P_2$, and (d)I-$Hf_3C_2Si_2$..

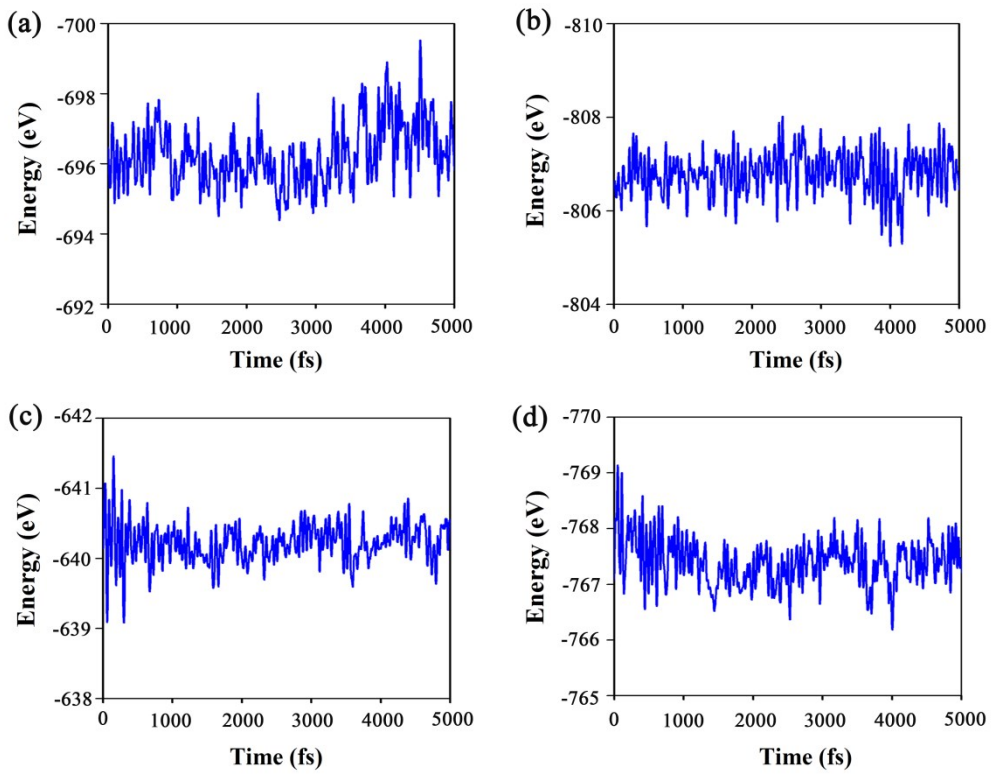

Fig. S2. Variation in free energy of (a) I-$Ti_3C_2Si_2$, (b) I-$Ti_3C_2P_2$, (c) I-$Ti_3C_2S_2$, and (d) I-$Ti_3C_2Cl_2$ over 5 ps during the AIMD simulation at 300 K.

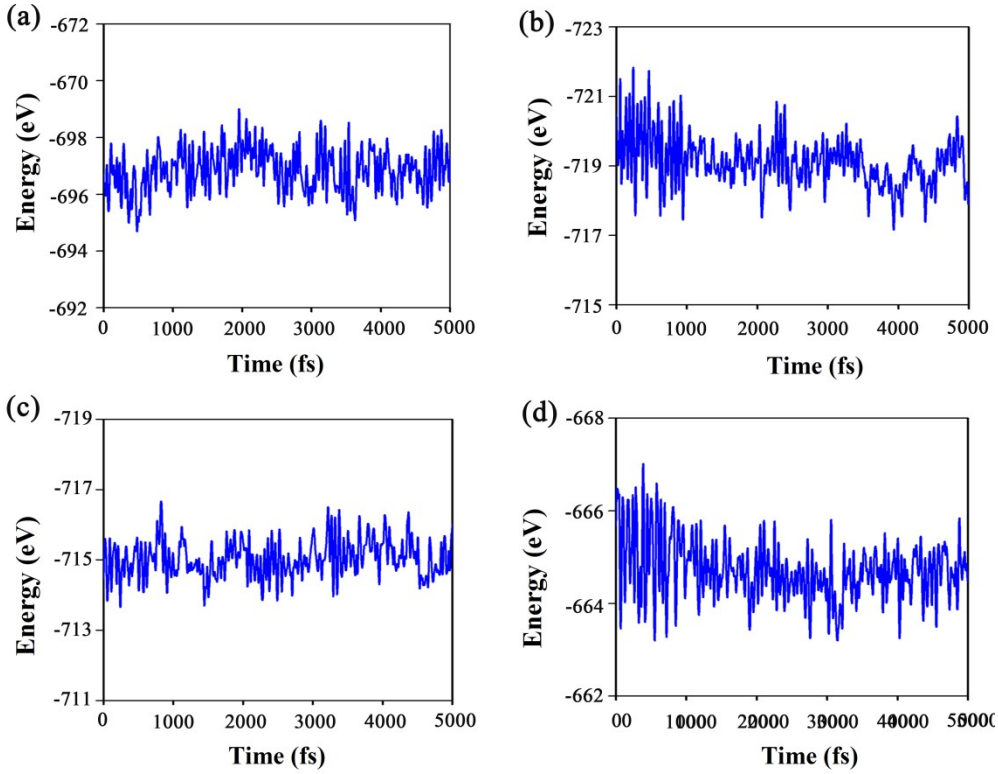

Fig. S3. Variation in free energy of (a) I-$Hf_3C_2Si_2$, (b) I-$Hf_3C_2P_2$, (c) I-$Hf_3C_2S_2$, and (d) I-$Hf_3C_2Cl_2$ over 5 ps during the AIMD simulation at 300 K.

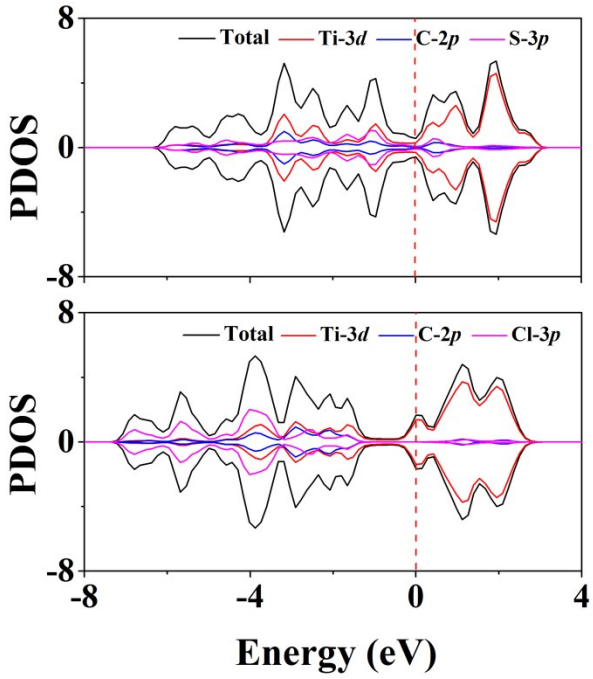

Fig. S4. The PDOS for (a) I-$Ti_3C_2S_2$ and (b) I-$Ti_3C_2Cl_2$. The Fermi level is set to zero.

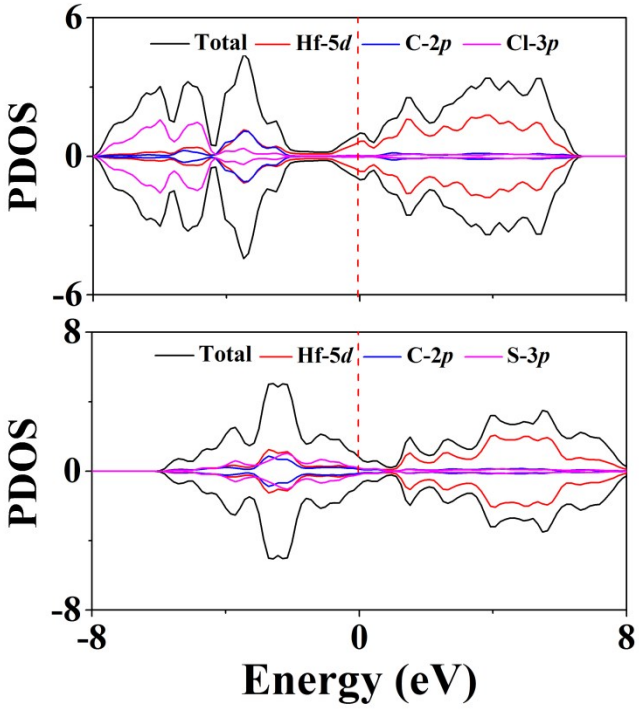

Fig. S5. The PDOS for (a) I-$Hf_3C_2S_2$ and (b) I-$Hf_3C_2Cl_2$. The Fermi level is set to zero.

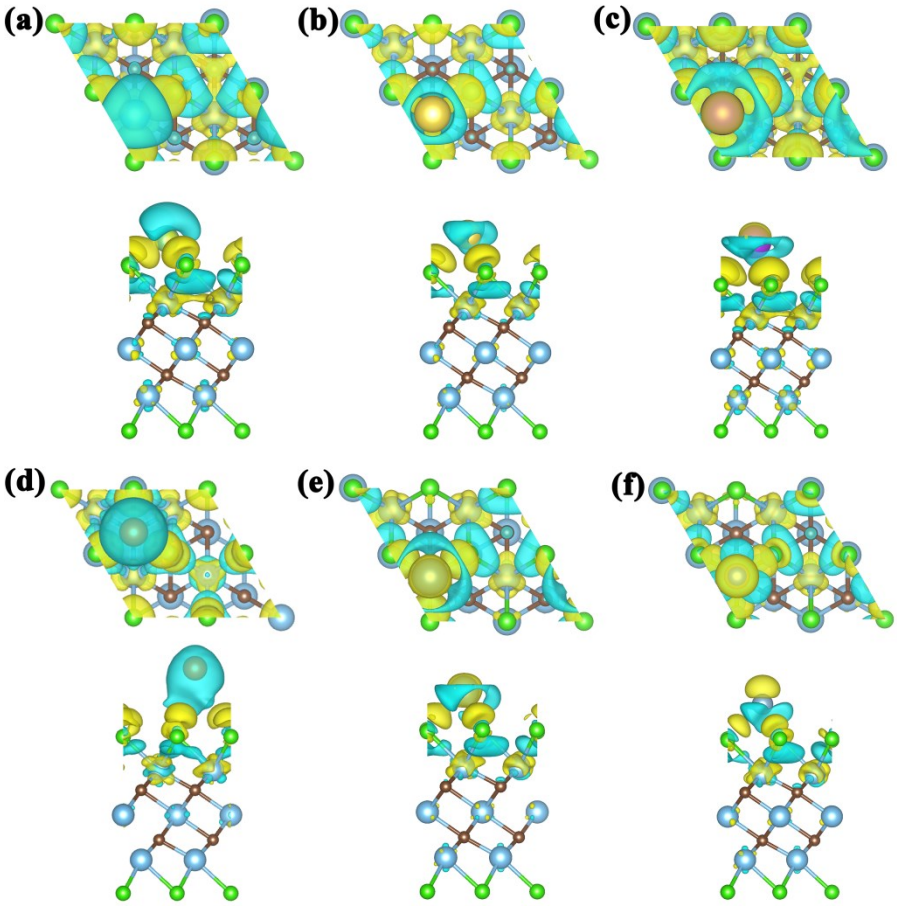

Fig. S6. Top and side view of charge density difference with Li, Na, K, Mg, Ca, Al adsorbed on the surface of $Ti_3C_2Cl_2$ (a, b, c, d, e, f), respectively, with the isosurface value of 0.0002 $Å^{-3}$. The yellow represents the charge sufficient, the blue represents the charge deficient.

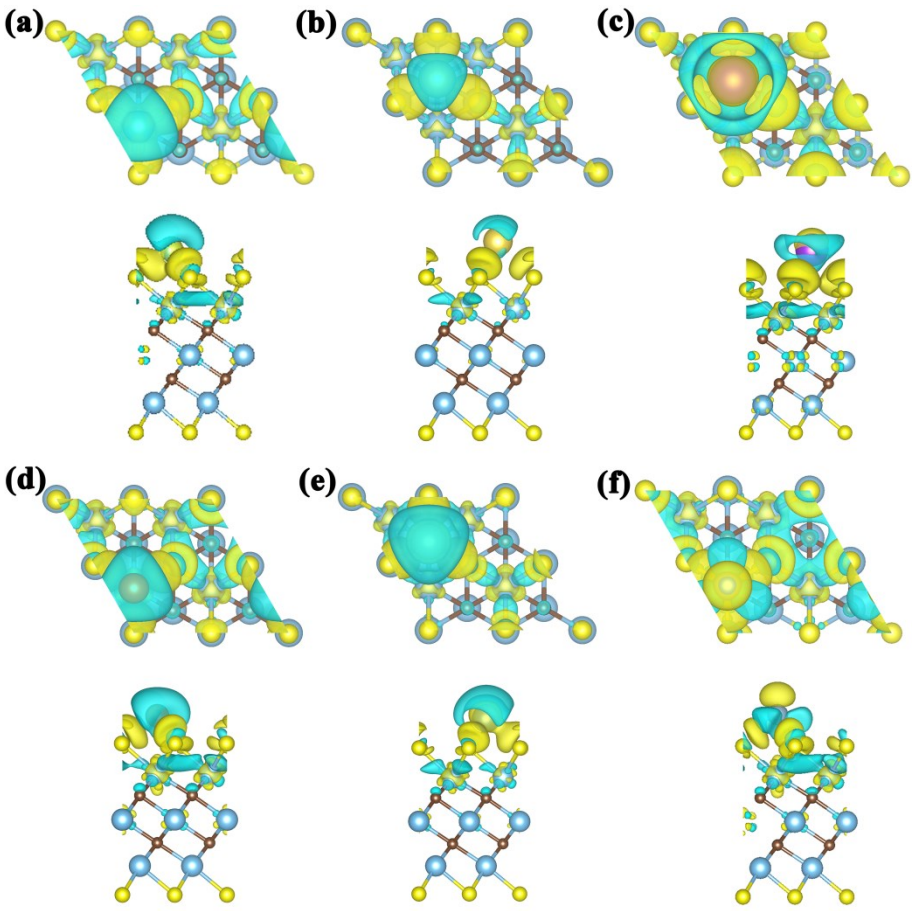

Fig. S7. Top and side view of charge density difference with Li, Na, K, Mg, Ca, Al adsorbed on the surface of $Ti_3C_2S_2$ (a, b, c, d, e, f), respectively, with the isosurface value of 0.0002 $Å^{-3}$. The yellow represents the charge sufficient, the blue represents the charge deficient.

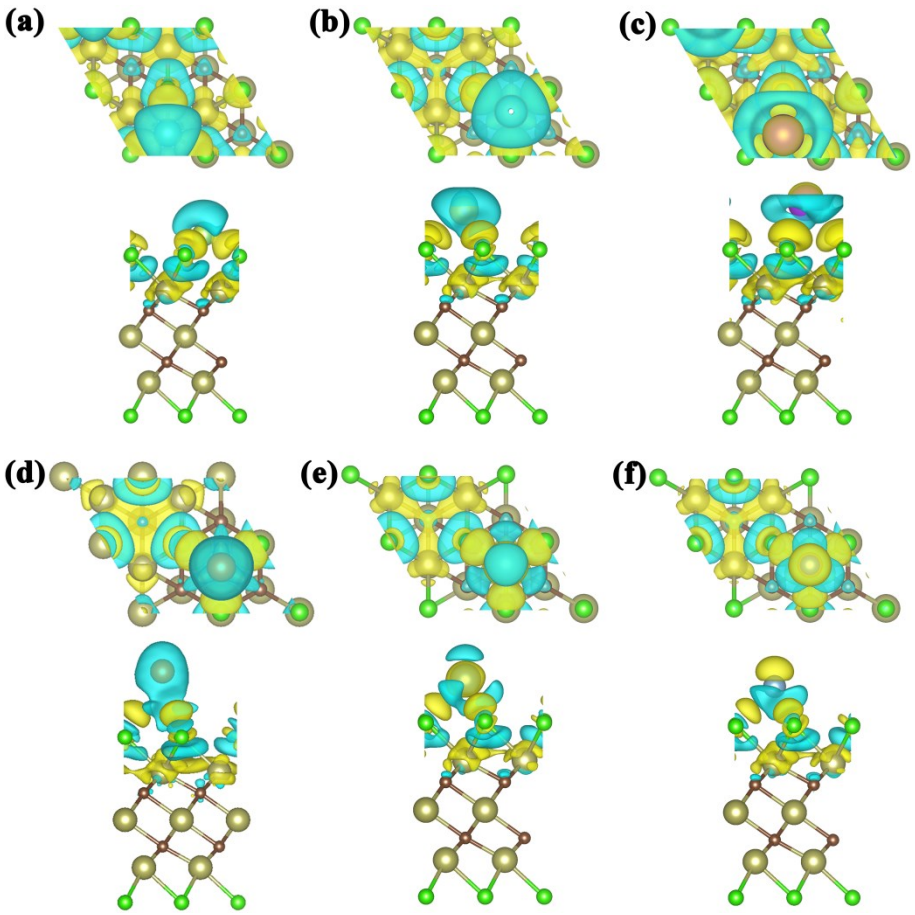

Fig. S8. Top and side view of charge density difference with Li, Na, K, Mg, Ca, Al adsorbed on the surface of $Hf_3C_2Cl_2$ (a, b, c, d, e, f), respectively, with the isosurface value of 0.0002 $Å^{-3}$. The yellow represents the charge sufficient, the blue represents the charge deficient.

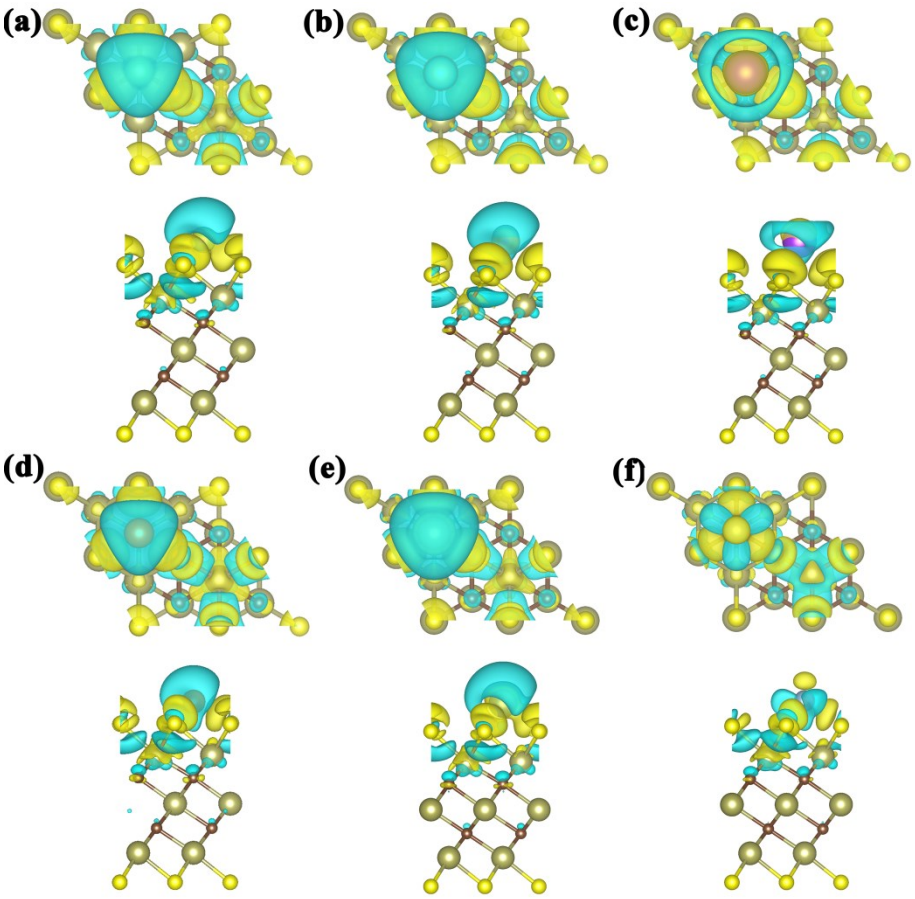

Fig. S9. Top and side view of charge density difference with Li, Na, K, Mg, Ca, and Al adsorbed on the surface of $Hf_3C_2S_2$ (a, b, c, d, e, f), respectively, with the isosurface value of 0.0002 $Å^{-3}$. The yellow represents the charge sufficient, the blue represents the charge deficient.

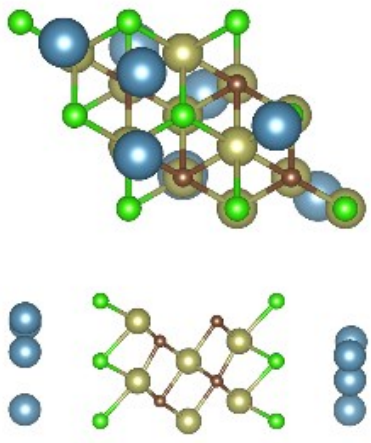

Fig. S10. The top and side views of $Hf_3C_2S_2Ca_2$ monolayer.

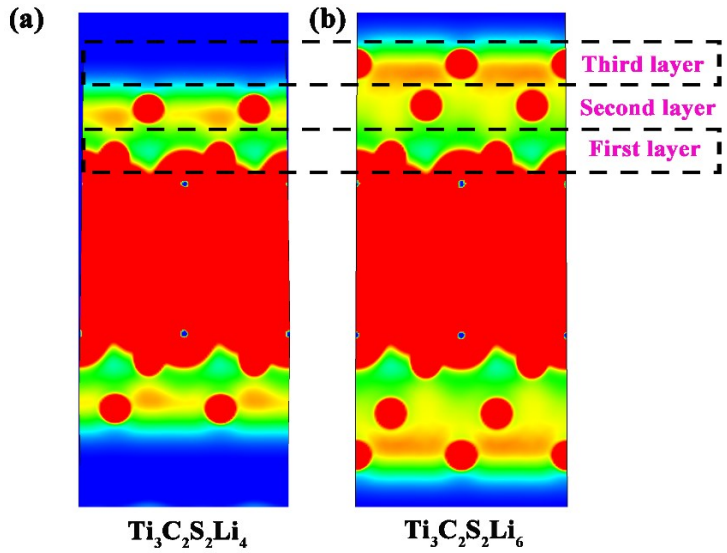

Fig. S11. The charge density map of $Ti_3C_2S_2$ monolayer (011) with (a) two-layer and (b) three-layer Li atoms.

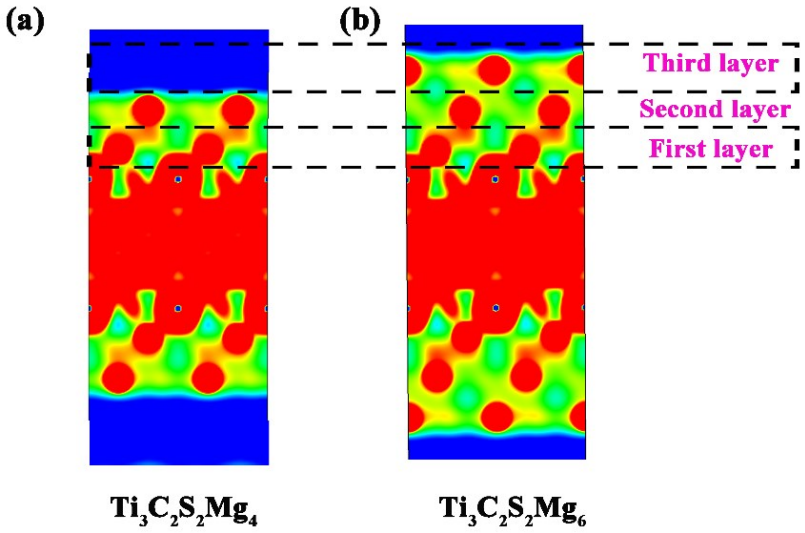

Fig. S12. The charge density map of $Ti_3C_2S_2$ monolayer (011) with (a) two-layer and (b) three-layer Mg atoms.

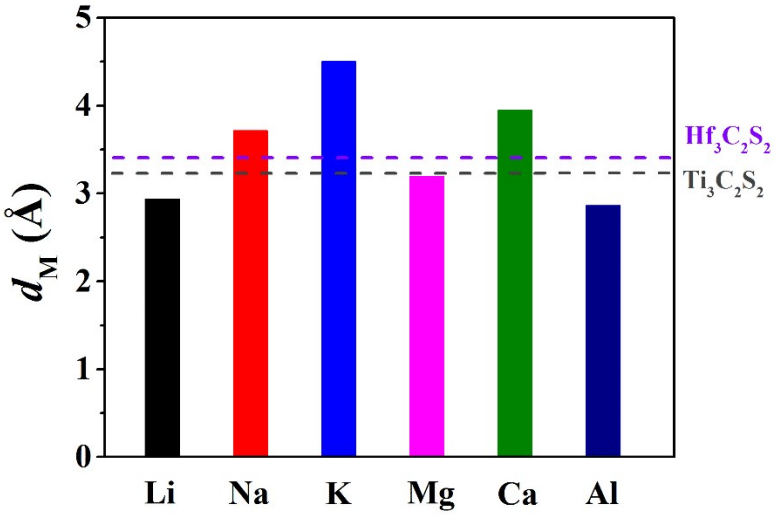

Fig. S13. Comparison of the metal diameters (d_M) with the lattice constants of $Ti_3C_2S_2$ and $Hf_3C_2S_2$ monolayer.

Supporting Tables

Table S1 The structure parameter of the optimized $Ti_3C_2X_2$ and $Hf_3C_2X_2$ monolayer.

	Parametera(Å)	Thickness d (Å)	Bond lengths (Å)		
			Ti/Hf(1)-C	Ti/Hf(2)-C	Ti/Hf(1)-T
Ti_3C_2	3.100	4.693	2.100	2.245	
I-$Ti_3C_2Si_2$	3.113	8.832	2.139	2.219	2.655
I-$Ti_3C_2P_2$	3.096	8.800	2.138	2.214	2.623
I-$Ti_3C_2S_2$	3.223	8.055	2.229	2.246	2.417
I-$Ti_3C_2Cl_2$	3.234	8.136	2.135	2.273	2.549
Hf_3C_2	3.284	5.078	2.211	2.358	
I-$Hf_3C_2Si_2$	3.276	9.265	2.255	2.339	2.774
I-$Hf_3C_2P_2$	3.369	8.671	2.282	2.373	2.639
I-$Hf_3C_2S_2$	3.390	8.418	2.357	2.367	2.505
I-$Hf_3C_2Cl_2$	3.377	8.855	2.228	2.389	2.658

Table S2 The surface energy (γ) and exfoliation energy (E_{exf}) of $Ti_3C_2X_2$ and $Hf_3C_2X_2$ (X = Si, P, S, and Cl).

	Ti_3C_2	$Ti_3C_2Si_2$	$Ti_3C_2P_2$	$Ti_3C_2S_2$	$Ti_3C_2Cl_2$
γ (J/m^2)	1.367	1.674	0.498	-0.796	-1.713
E_{exf} (J/m^2)	3.761	4.717	1.007	0.169	0.140
	Hf_3C_2	$Hf_3C_2Si_2$	$Hf_3C_2P_2$	$Hf_3C_2S_2$	$Hf_3C_2Cl_2$
γ (J/m^2)	-0.491	-0.010	-1.524	-2.926	-3.669
E_{exf} (J/m^2)	1.992	2.050	1.241	0.202	0.087

Table S3. The binding energy (E_b) at different adsorption sites of metal atom on the $Ti_3C_2S_2$, $Ti_3C_2Cl_2$, $Hf_3C_2S_2$, and $Hf_3C_2Cl_2$ monolayer.

		Li	Na	K	Mg	Ca	Al
$Ti_3C_2S_2$	C site	-3.524	-2.716	-2.734	-2.194	-4.116	-3.364
	Ti site	-3.562	-2.715	-2.717	-2.211	-3.990	-3.395
$Ti_3C_2Cl_2$	C site	-2.013	-1.098	-1.201	-0.219	-1.290	-1.316
	Ti site	-2.024	-1.101	-1.209	-0.216	-1.329	-1.371
$Hf_3C_2S_2$	C site	-3.968	-3.251	-3.326	-3.089	-5.039	-3.992
	Ti site	-3.926	-3.191	-3.282	-2.979	-4.838	-3.877

$Hf_3C_2Cl_2$	C site	-1.407	-0.677	-0.917	-0.188	-0.630	-0.700
	Ti site	-1.393	-0.689	-0.881	-0.190	-0.657	-0.756

Table S4. The most stable adsorption site of metal atom on the monolayer.

	Li	Na	K	Mg	Ca	Al
$Hf_3C_2S_2$	C	C	C	C	C	C
$Hf_3C_2Cl_2$	C	$T_M(1)$	C	$T_M(1)$	$T_M(1)$	$T_M(1)$
$Ti_3C_2S_2$	$T_M(1)$	C	C	$T_M(1)$	C	$T_M(1)$
$Ti_3C_2Cl_2$	$T_M(1)$	$T_M(1)$	$T_M(1)$	C	$T_M(1)$	$T_M(1)$

Table S5. Charge transfer (|e|) from metal to I-$T_{M3}C_2X_2$ monolayer by Bader charge analysis.

	Li	Na	K	Mg	Ca	Al
$Ti_3C_2S_2$	0.885	0.850	0.821	1.351	1.337	1.034
$Ti_3C_2Cl_2$	0.892	0.694	0.615	0.098	0.902	0.845
$Hf_3C_2S_2$	0.880	0.867	0.842	1.572	1.401	1.358
$Hf_3C_2Cl_2$	0.884	0.616	0.567	0.076	0.783	0.736

Table S6. Diffusion barrier energies (eV) of M on the I-$T_{M3}C_2X_2$ monolayers surface.

	Li	Na	K	Mg	Ca	Al
$Ti_3C_2S_2$	0.224	0.125	0.093	0.354	0.370	0.189
$Ti_3C_2Cl_2$	0.250	0.081	0.042	0.002	0.144	0.114
$Hf_3C_2S_2$	0.237	0.162	0.132	0.543	0.527	0.289
$Hf_3C_2Cl_2$	0.198	0.060	0.049	0.006	0.081	0.056

Table S7 The calculated layer-by-layer adsorption energy ($E_{layer\text{-}n}$) $Ti_3C_2S_2$ monolayer.

	E_{ad}/single (eV)	$E_{layer\text{-}1}$(eV)	$E_{layer\text{-}2}$(eV)	$E_{layer\text{-}3}$(eV)
Li	-1.92	-0.97	-0.0036	-0.028
Na	-1.63	-0.60	-0.0085	

K	-1.97	-0.12	-0.37	
Mg	-0.76	-0.27	-0.095	-0.015
Ca	-2.09	-0.32	0.55	
Al	-0.07	0.35		

Table S8 The calculated layer-by-layer adsorption energy ($E_{layer\text{-}n}$) on the $Ti_3C_2Cl_2$ monolayer.

	$E_{layer\text{-}1}$(eV)
Li	0.21
Na	0.12
K	0.75
Mg	0.47
Ca	0.75
Al	1.13

Table S9 The calculated layer-by-layer adsorption energy ($E_{layer\text{-}n}$) $Hf_3C_2S_2$ monolayer.

	E_{ad}/single (eV)	$E_{layer\text{-}1}$(eV)	$E_{layer\text{-}2}$(eV)	$E_{layer\text{-}3}$(eV)
Li	-2.26			
Na	-2.07	-0.87	-0.054	
K	-2.46	-0.68		
Mg	-1.25	-0.36	-0.08	
Ca	-2.78	-0.93	-0.13	0.21
Al	-0.42	0.35		

Table S10 The calculated layer-by-layer adsorption energy ($E_{layer\text{-}n}$) $Hf_3C_2Cl_2$ monolayer.

	$E_{layer\text{-}1}$(eV)
Li	0.42
Na	0.15
K	0.58
Mg	0.58
Ca	-1.72
Al	1.11

Table S11. Comparisons of different layered MXene materials, with their respective storage capacities and energy barriers as Li-ion batteries

	Energy barrier/eV	Storage capacity/mA h g^{-1}	Ref.
$Ti_3C_2S_2$	0.22	462.68	This work
$Hf_3C_2S_2$	0.24	85.97	
Ti_2CP_2	0.32	1264	[3]
V_2CP_2	0.26	1220	[3]

Ti_2CSi_2	0.29	1767	[3]
V_2CSi_2	0.23	1592	[3]
Ti_2CS_2	0.22	311.86	[4]
V_2NS_2	0.17	299.52	[5]
Ti_2NS_2	0.19	308.28	[5]
Zr_2CO_2	0.49	266	[6]
Zr_2CS_2	0.22	259	[6]
$Ti_3C_2F_2$	0.36	130	[7]
$Ti_3C_2(OH)_2$	0.90	67	[7]
$Hf_3C_2F_2$	0.225	80.74	[8]
$Hf_3C_2(OH)_2$	0.440	162.57	[8]

Table S12. Comparisons of different layered MXene materials, with their respective storage capacities and energy barriers as Na-ion batteries

	Energy barrier/eV	Storage capacity/mA h g^{-1}	Ref.
Ti_2CS_2	0.11	935	[4]
$Ti_3C_2O_2$	0.22	463	[9]
Zr_2CO_2	0.29	474	[10]
$Zr_3C_2O_2$	0.32	326	[10]

Table S13. Comparisons of energy barriers, storage capacities, and OCV of layered MXenes as Mg-ion batteries.

	Energy barrier/eV	Storage capacity/mA h g^{-1}	OCV/V	Ref.
$Ti_3C_2S_2$	0.354	1388	0.13	This work
Ti_2CS_2	0.46	1871	0.10	[4]
TiS_2	0.55	957	0-0.5	[11]
Ti_2CO_2	0.71	570	--	[12]
C_2N	0.04	1175	0.45	[13]

Table S14 The number of adsorption layers of metal atoms in different 2D materials.

	Li	Na	K	Mg	Ca	Al
$Ti_3C_2S_2$	2	2	1	3	1	0
$Hf_3C_2S_2$	1	2	1	2	2	0

Table S15. Coordinates corresponding to the most stable structure.

Phase	Lattice Parameters	Coordinates
$Ti_3C_2S_2$	a = b = 3.219 Å	C1 (1.609, 0.929, 19.801)
	$\alpha = \gamma = 90.000$ °	C2 (0.000, 1.858, 17.275)

	β = 120.000 º	Ti1 (1.609, 0.929, 16.048) Ti2 (0.000, 1.858, 21.028) Ti3 (0.000, -0.000, 18.538) S1 (0.000, 0.0000, 22.576) S2 (1.609, 2.788, 14.500)
$Ti_3C_2Cl_2$	a = b = 3.235 Å $\alpha = \gamma$ = 90.000 º β = 120.000 º	C1 (1.618, 0.939, 17.110) C2 (0.000, 1.872, 14.516) Ti1 (1.618, 0.938, 13.480) Ti2 (0.001, 1.873, 18.149) Ti3 (0.000, 0.005, 15.813) Cl1 (1.617, 2.806, 19.880) Cl2 (0.000, 0.004, 11.746)
$Hf_3C_2S_2$	a = b = 3.390 Å $\alpha = \gamma$ = 90.000 º β = 120.000 º	C1 (1.695, 0.9786, 20.575) C2 (-0.000, 1.957, 17.907) Hf1 (-0.000, 0.000, 19.241) Hf2 (-0.000, 1.957, 21.888) Hf3 (1.695, 0.979, 16.594) S1 (-0.000, 0.000, 23.453) S2 (-0.000 0.000, 15.030)
$Hf_3C_2Cl_2$	a = b = 3.371 Å $\alpha = \gamma$ = 90.000 º β = 120.000 º	C1 (1.686, 0.973, 16.399) C2 (0.000, 1.946, 13.615) Hf1 (0.000, 0.000, 15.007) Hf2 (0.000, 1.946, 17.476) Hf3 (1.686, 0.973, 12.538) Cl1 (0.000, 0.000, 19.284) Cl2 (0.000, 0.000, 10.730)

References

1. Y. Han, K. C. Lai, A. Lii-Rosales, M. C. Tringides, J. W. Evans and P. A. Thiel, Surface energies, adhesion energies, and exfoliation energies relevant to copper-graphene and copper-graphite systems *Surf. Sci.* 2019, **685**, 48-58.
2. P. L. Gong, F. Zhang, L. F. Huang, H. Zhang, L. Li, R. C. Xiao, B. Deng, H. Pan and X. Q. Shi, Multifunctional two-dimensional semiconductors SnP_3: universal mechanism of layer-dependent electronic phase transition, *J. Phys.: Condens. Matter* 2018, **30**, 475702.
3. J. Zhu and U. Schwingenschlögl, P and Si functionalized MXenes for metal-ion battery applications, *2D Mater.* 2017, **4**, 025073.
4. Y. Wang, M. Zhou, L.-C. Xu, W. Zhao, R. Li, Z. Yang, R. Liu and X. Li, Achieving superior high-capacity batteries with the lightest Ti_2C MXene anode by frst-principles calculations: Overarching role of S-functionate (Ti_2CS_2) and multivalent cations, carrier *J. Power Sources* 2020, **451**, 227791.

5. V. Shukla, N. K. Jena, S. R. Naqvi, W. Luo and R. Ahuja, Modelling high-performing batteries with Mxenes: The case of Sfunctionalized two-dimensional nitride Mxene electrode, *Nano Energy* 2019, **58**, 877-885.
6. J. Zhu, A. Chroneos, J. Eppinger and U. Schwingenschlögl, S-functionalized MXenes as electrode materials for Li-ion batteries, *Appl. Mater. Today* 2016, **5**, 19-24.
7. Q. Tang, Z. Zhou and P. Shen, Are MXenes Promising Anode Materials for Li Ion Batteries? Computational Studies on Electronic Properties and Li Storage Capability of Ti_3C_2 and $Ti_3C_2X_2$ (X = F, OH) Monolayer *J Am. Chem. Soc*. 2012, **134**, 16909-16916.
8. Z. Yang, Y. Zheng, W. Li and J. Zhang, Investigation of Two-Dimensional Hf-Based MXenes as the Anode Materials for Li/Na-Ion Batteries: A DFT Study. *J. Comput. Chem.* 2019, **40**, 1352-1359.
9. Q. Meng, J. Ma, Y. Zhang, Z. Li, C. Zhi, A. Hu and J. Fan, The S-functionalized Ti_3C_2 Mxene as a High Capacity Electrode Material for Na-ion Batteries: A DFT Study, *Nanoscale* 2018, **10**, 3385-3392.
10. Q. Meng, J. Ma, Y. Zhang, Z. Li, A. Hu, J.-J. Kai and J. Fan, Theoretical investigation of zirconium carbide MXenes as prospective high capacity anode. *J. Mater. Chem. A* 2018, **6**, 13652-13660.
11. A. Samad, A. Shafique, Y. H. Shin, Adsorption and diffusion of mono, di, and trivalent ions on two-dimensional TiS2. *Nanotechnology* 2017, **28**, 175401.
12. Y. Xie, Y. Dall'Agnese, M. Naguib, Y. Gogotsi, M. W. Barsoum, H. L. Zhuang, P. R. C. Kent, Prediction and Characterization of MXene Nanosheet Anodes for Non-Lithium-Ion Batteries. *ACS Nano* 2014, **8**, 9606-9615.
13. D. Wu, B. Yang, H. Chen, E. Ruckenstein, Mechanical deformation induced charge redistribution to promote the high performance of stretchable magnesium-ion batteries based on two-dimensional C_2N anodes. *Nanoscale* 2019, **11**, 15472-15478.